Organic-Ru²⁺ Cluster Initiated Dendritic-faced Metallo-Octahedron and Its Unpredictable Photoactivity

Zhiyuan Jiang,[a] Tun Wu,[b*] Yiming Li,[a*] Jun Wang,[a] Mingzhao Chen,[b] PeiYang Su,[b] Zhe Zhang,[b] Ting-Zheng Xie[b] and Pingshan Wang[a,b*]

Table of Content

1. General Procedures

All starting materials were purchased from Aldrich, Alfa Aesar and used without further purification. Compound 4'-Boronatopenyl[2,2':6',2''[terpyridine and [1,2-methoxy-4,5-bis(4'-benzene-4'-tripyridine]benzene were synthesized according to the reported methods[S1]. Column chromatography was conducted by using basic Al_2O_3 (sinopharm chemical reagents co., Ltd, 200-300 mesh) or SiO_2 (Qingdao Haiyang Chemical co., Ltd, 200-300 mesh). The ^{1}H NMR and ^{13}C NMR spectra were recorded on a Bruker Avance 400 MHz and 500 MHz NMR spectrometer in $CDCl_3$, CD_3OD and CD_3CN with TMS as the inner standard. Electro-spray ionization (ESI) mass spectra were recorded with a Bruker Q-TOF Qualification Standard Kit., using solutions of 0.1 mg sample in 10 mL of $CHCl_3$/ CH_3CN (1:3, v/v) for ligands or 1 mg in 5 mL of CH_3CN or CH_3CN/CH_3OH (3:1, v/v) for complexes. Electron spin-resonance (ESR) spectra were recorded on a Bruker E-500 magnetic resonance instrument at room temperature. Singlet oxygen was generated from Perfect Light PCX-50A Discover (power density was 80 mW/cm^2). UV-vis diffuse reflectance data were recorded with a Hitachi UH4150 spectrophotometer.

Transmission Electron Microscopy (TEM): The sample was dissolved in CH_3CN at a concentration of ~10^{-7} M. The solutions were dropped cast onto a carbon-coated Cu grid (300-400 mesh) and extra solution was absorbed by filter paper to avoid aggregation. The TEM images of the drop cast samples were taken with a JEOL 2010 and JEOL JEM-2800 Transmission Electron Microscope.

Molecular Modeling. Energy-minimized structures were obtained following the same settings in the literature[S2]. Calculations were proceeded with Anneal and Geometry Optimization functions in Forcite module of Materials Studio version 6.1 program (Accelrys Software, Inc.).

2. Experimental section
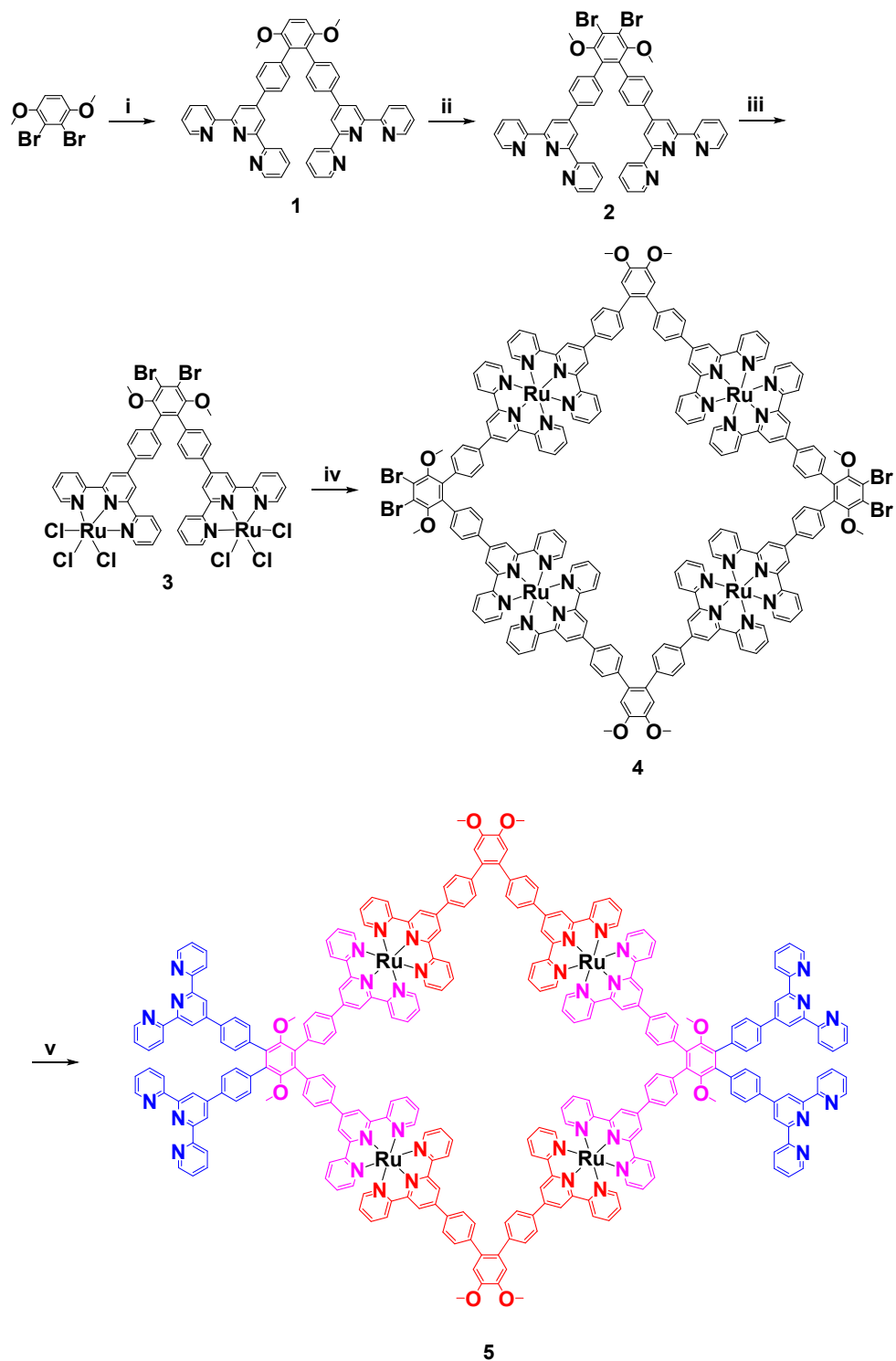
Scheme S1: Synthesis of the ligand **5**. Reagents and conditions: (i) Tpy-B(OH)$_2$, THF, Pd(PPh$_3$)$_4$, NaOH, refluxed, 2 d; (ii) CHCl$_3$, Br$_2$, refluxed 2 d; (iii) RuCl$_3$·3H$_2$O, EtOH, refluxed, 2 d; (iv) CHCl$_3$: CH$_3$OH (1 : 2, v : v), [1,2-methoxy-4,5-bis(4'-benzene-4'-tripyridine]benzene, N-ethylmorpholine, refluxed, 2 d; (v) Tpy-B(OH)$_2$, Pd(PPh$_3$)$_4$, Na$_2$CO$_3$, CH$_3$CN, refluxed, 4 d.
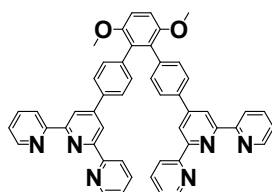
1

1: 2,3-Bis(4'-terpyridyl-p-phenyl) -1,4-dimethoxybenzene were prepared through a single-pot reaction: 2,3-Dibromo-1,4-dimethoxybenzene (592 mg, 2 mmol), 4'-(4-boronatophenyl)-2,2':6',2''-terpyridine (1.42 g, 4 mmol) in THF (160 mL), aqueous NaOH (480 mg, 12 mmol) (1 M) was added. The system was degassed for 10 minutes, then Pd(PPh$_3$)$_4$ (231 mg) was added. After refluxing for 2 days under N$_2$. The solvent was removed in vacuo to give a residue that was dissolved in CHCl$_3$ and washed with water. The organic layer was dried (anhydrous MgSO$_4$), concentrated in vacuum to give a residue that was purified by flash column chromatography (Al$_2$O$_3$) eluting with CHCl$_3$ to give compound **1**, as white solid: 1.2 g (Yield: 80%); m.p. = 287 °C; ^{1}H NMR (400 MHz, CDCl$_3$, 298 K) δ: 8.69 (s, 4H, Tpy-$H^{3',5'}$), 8.66-8.65 (d, J= 4 Hz, 4H, Tpy-$H^{6,6''}$), 8.62-8.60 (d, J= 8 Hz, 4H, Tpy-$H^{3,3''}$), 7.85-7.80 (t, J= 10 Hz, 4H, Tpy-$H^{4,4''}$), 7.77-7.75 (d, J= 8 Hz, 4H, Ph-H^j), 7.31-7.27 (t, J= 8 Hz, 4H, Tpy-$H^{5,5''}$),7.25-7.23 (d, J= 8 Hz, 4H, Ph-H^k), 7.02(s, 2H, Ph-H^a), 3.77 (s, 6H, -OCH$_3$); ^{13}C NMR (101 MHz, CDCl$_3$, 298 K) δ: 156.40, 155.77, 151.45, 150.03, 149.07, 137.70, 136.73, 136.18, 131.85, 131.47, 126.40,123.62, 121.30, 118.89, 111.36; ESI/MS (*m/z*): Calcd. For: 753.30 [M+H]$^+$, Found For: 753.26 [M+H]$^+$.
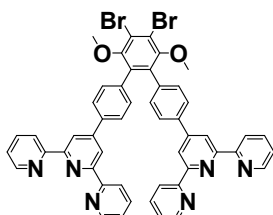

2

2: Structure of **1** (752 mg, 1 mmol) was dissolved in 100 mL CHCl$_3$, Br$_2$ (3.2 g, 20 mmol) was added to the solution slowly under stirring, then the mixture was heated to reflux for 2 days, with a tube to absorb the HBr gas, when the solution became colorless, the mixture was cooled to room temperature and poured into cold NaHSO$_3$ aqueous solution, then extracted with DCM for 3 times (200 mL*3), the organic phase was combined and washed wit brine and purified on column, eluting with DCM as a eluent, 820 mg target compound **2** was obtained as a white solid (yield: 90%); m.p. > 300°C. ^{1}H NMR (400 MHz, CDCl$_3$, 298 K) δ: 8.70 (s, 4H, Tpy-H3',5'), 8.67-8.66 (d, J= 4 Hz, 4H, Tpy-$H^{6,6''}$), 8.64-8.62 (d, J= 8.0 Hz, 4H, Tpy-$H^{3,3''}$), 7.87-7.83 (t, J= 8 Hz, 4H, Tpy-$H^{4,4''}$), 7.79-7.77 (d, J= 8 Hz, 4H, Ph-H^j), 7.33-7.30 (t, J= 6 Hz, 4H, Tpy-$H^{5,5''}$), 7.29-7.26 (d, J= 12 Hz, 4H, Ph-H^k), 3.41 (s, 6H, -OCH$_3$); ^{13}C NMR (101 MHz, CDCl$_3$, 298 K) δ: 156.23, 155.87, 152.53, 149.71, 149.06, 137.19, 136.83, 136.18, 135.70, 131.21, 126.77, 123.76, 121.33, 118.90; ESI/MS (*m/z*): Calcd [M+H]$^+$: 911.12, Found [M+H]$^+$: 911.12.

3
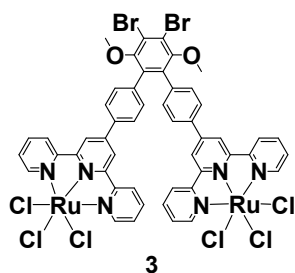
3: Compound **2** (910.7 mg, 1.00 mmol) and RuCl₃·3H₂O (522.9 mg, 2.00 mmol) was suspended in EtOH (60 mL). After stirred for 8 h at room temperature, the mixture was heated up to 75°C and stirred for 2 d, then cooled to 25 °C and filtered to obtain a brown powder. The solid was washed with MeOH repeatedly until the filtrate gets clean and colorless, the solid was collected and dried in vacuum for 12 h to get the desired compound, it was used directly for the next step without further purification: 1.07 g, (yield: 81%).
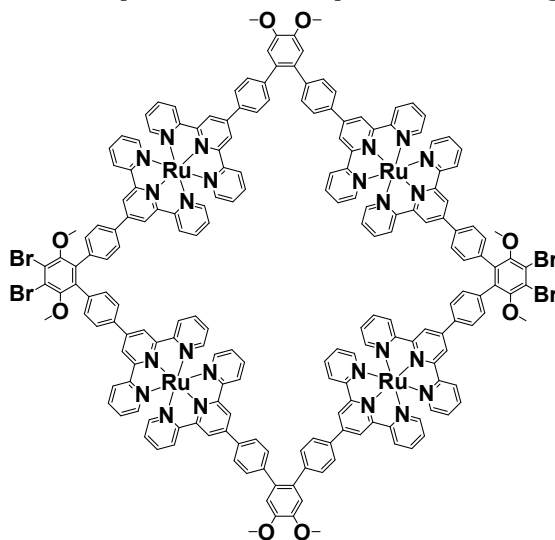
4: A mixture of ligand **3** (662.8 mg, 0.5 mmol) and [1,2-methoxy-4,5-bis (4'-benzene-4'-tripyridine] benzene (376.4 mg 0.5 mmol) was added to a 500 mL flask, then CH₃OH (200 mL) and CHCl₃ (100 mL) was added, after added 4 drops of 4-Ethylmorpholine, the mixture was stirred at 75 °C for 2 days, After cooled to ambient temperature then concentrated in vacuo followed by column chromatography (Al₂O₃) eluting with the mixture of CH₃OH and CH₂Cl₂ (4.5:100) to generate a pure product as red solid: 320.0 mg, (yield: 32%); m.p. > 300°C. ^{1}H NMR (500 MHz, CD₃OD, 298 K) δ: 9.27 (s, 16H, Tpy-$H^{3',5'}$), 8.87-8.86 (d, J= 5 Hz, 16H, Tpy-$H^{3,3''}$), 8.28-8.24 (m, 16H, Ph-H^j), 7.96-7.93 (t, J= 7.5 Hz, 16H, Tpy-$H^{4,4''}$), 7.65-7.63 (m, 16H, Ph-H^k), 7.50-7.47 (m, 16H, Tpy-$H^{6,6''}$), 7.24-7.20 (m, 20H, Tpy-$H^{5,5''}$, Ph-H^a), 4.02 (s, 12H, -OCH₃), 3.55 (s, 12H, -OCH₃); ^{13}C NMR (101 MHz, CD₃OD, 298 K) δ: 159.47, 157.00, 156.94, 154.13, 153.31, 150.69, 149.82, 149.51, 145.39, 139.48, 137.25, 137.07, 136.12, 133.85, 133.37, 132.55, 129.01, 128.79, 128.47, 128.45, 126.18, 122.73, 122.54, 115.62, 79.73, 61.35, 57.71, 57.42, 56.91, 32.57, 21.42; ESI-MS (*m/z*): [M-5Cl⁻]⁵⁺ (*m/z* = 767.74) (Calcd. *m/z* = 767.50), [M-4Cl⁻]⁴⁺ (*m/z* = 968.40) (Calcd. *m/z* = 968.25), [M-3Cl⁻]³⁺ (*m/z* = 1303.18) (Calcd. *m/z* = 1302.83).
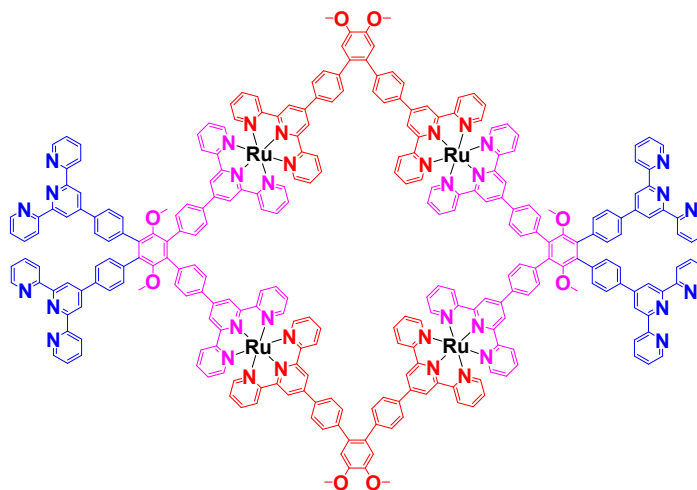
5: To a solution of (4-[2,2':6',2''-terpyridin-4'-ylphenyl)boronic acid (127.1mg, 0.36 mmol) and compound **4** (60.2 mg, 0.015 mmol)in CH₃CN (60 mL), aqueous K₂CO₃ (41.5 mg, 0.3 mmol) (1M) was added. The system was degassed for 10 min, then Pd(PPh₃)₄ (20.8 mg, 0.018 mmol) was added. After refluxing for 4 d under N₂, the solvent was removed in vacuo to give a residue that was purified by flash column chromatography (Al₂O₃) eluting with CH₂Cl₂:CH₃OH (100:4.25) to give compound **5**, as red solid: 57.2 mg (55%). ¹H NMR (500 MHz, CD₃CN, 298 K) δ: 9.05 (s, 8H, Tpy-*H*ᵦ³',⁵'), 9.01 (s, 8H, Tpy-*H*ₐ³',⁵'), 8.81-8.75 (m, 24H, Tpy-*H*꜀³',⁵', Tpy-*H*꜀⁶,⁶'', Tpy-*H*꜀³,³''), 8.68-8.66 (d, *J*= 10 Hz, 8H, Tpy-*H*ᵦ³,³''), 8.64-8.62 (d, *J*= 10 Hz, 8H, Tpy-*H*ᵦ³,³''), 8.25-8.16 (m, 24H, Ph-*H*ₐ,ᵦ,꜀ʲ), 7.96-7.94 (d, *J*= 10 Hz, 8H, Tpy-*H*꜀⁴,⁴''), 7.90-7.86 (m, 16H, Tpy-*H*ₐ,ᵦ⁴,⁴''), 7.80-7.65 (m, 24H, Ph-*H*ₐ,ᵦ,꜀ᵏ), 7.61-7.60 (d, *J*= 5 Hz, 8H, Tpy-*H*꜀⁵,⁵''), 7.39-7.38 (d, *J*= 5 Hz, 16H, Tpy-*H*ₐ,ᵦ⁶,⁶''), 7.20 (s, 4H, Ph-*H*ₐᵇ), 7.13-7.07 (m, 16H, Tpy-*H*ₐ,ᵦ⁵,⁵''), 4.00 (s, 12H, A-OCH₃), 3.16 (s, 12H, B-OCH₃). ¹³C NMR (101 MHz, CD₃CN, 298 K) δ 158.51, 155.93, 149.81, 138.51, 131.85, 127.95, 124.97, 122.05, 118.82, 78.34, 66.30, 56.30; ESI-MS (*m/z*): [M-7NTf₂⁻]⁷⁺ (*m/z* = 703.78) (Calcd. *m/z* = 703.62), [M-6NTf₂⁻]⁶⁺ (*m/z* = 867.73) (Calcd. *m/z* = 867.58), [M-5NTf₂⁻]⁵⁺ (*m/z* = 1097.27) (Calcd. *m/z* = 1097.17), [M-4NTf₂⁻]⁴⁺ (*m/z* = 1441.52) (Calcd. *m/z* = 1441.44), [M-3NTf₂⁻]³⁺ (*m/z* = 2012.65) (Calcd. *m/z* = 2015.29).
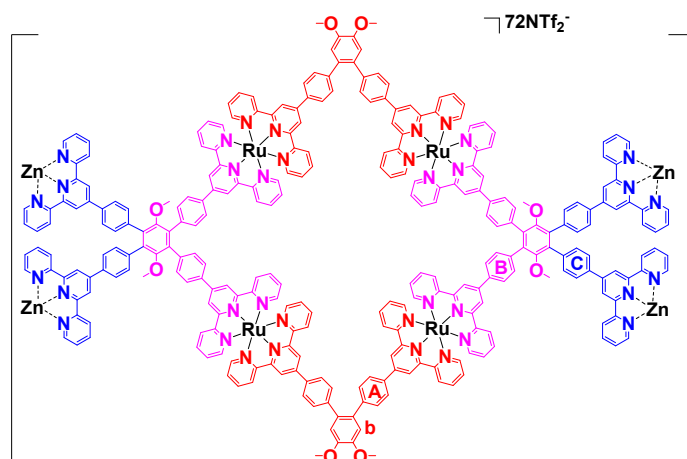
the dendritic-faced metallo-octahedron **6:** To a solution of ligand **5** (4.8 mg, 0.70 μmol) in acetonitrile (10 mL), a CH₃OH (2 mL) solution of Zn(NTf₂)₂ (0.87 mg, 1.39μmol) was slowly added. Under 60 °C for 12 h, after cooled to room temperature, excess LiNTf₂ in MeOH was added to get a red precipitate, which was filtered and washed with CH₃OH, and

then dried *in vacuo* to give (95%) the complex **6**, as a red solid. ^{1}H NMR (500 MHz, CD$_3$CN, 298 K) δ: 9.05-9.00 (m, 144H, tpy-H$^{3',5'}$), 8.75-8.70 (m, 48H, tpy-H$_\text{C}^{3,3''}$), 8.66-8.61 (m, 96H, tpy-H$_\text{A,B}^{3,3''}$), 8.28-8.26 (d, 48H, *J*=10 Hz, Ph-H$_\text{C}^\text{j}$), 8.21-8.16 (m, 96H, Ph-H$_\text{A,B}^\text{j}$), 8.09-8.06 (t, 48H, *J*= 7.5 Hz, tpy-H$_\text{C}^{4,4''}$), 7.88-7.80 (m, 240H, tpy-$H_\text{A,B}^{4,4''}$, tpy-$H_\text{C}^{6,6''}$, Ph-$H_\text{B,C}^\text{k}$), 7.68-7.64 (m, 48H, Ph-H_A^k), 7.38-7.34 (m, 144H, tpy-$H_\text{A,B}^{6,6''}$, tpy-$H_\text{C}^{5,5''}$), 7.22-7.20 (d, *J*= 10 Hz, 48H, Ph-H_A^b), 7.13-7.06 (m, 96H, tpy-$H_\text{A,B}^{5,5''}$), 4.01 (s, 72H, A-OCH$_3$), 3.22 (s, 72H, B-OCH$_3$). ESI-MS (*m/z*): Table S2.

3. NMR spectra of ligands and the dendritic-faced metallo-octahedron 6
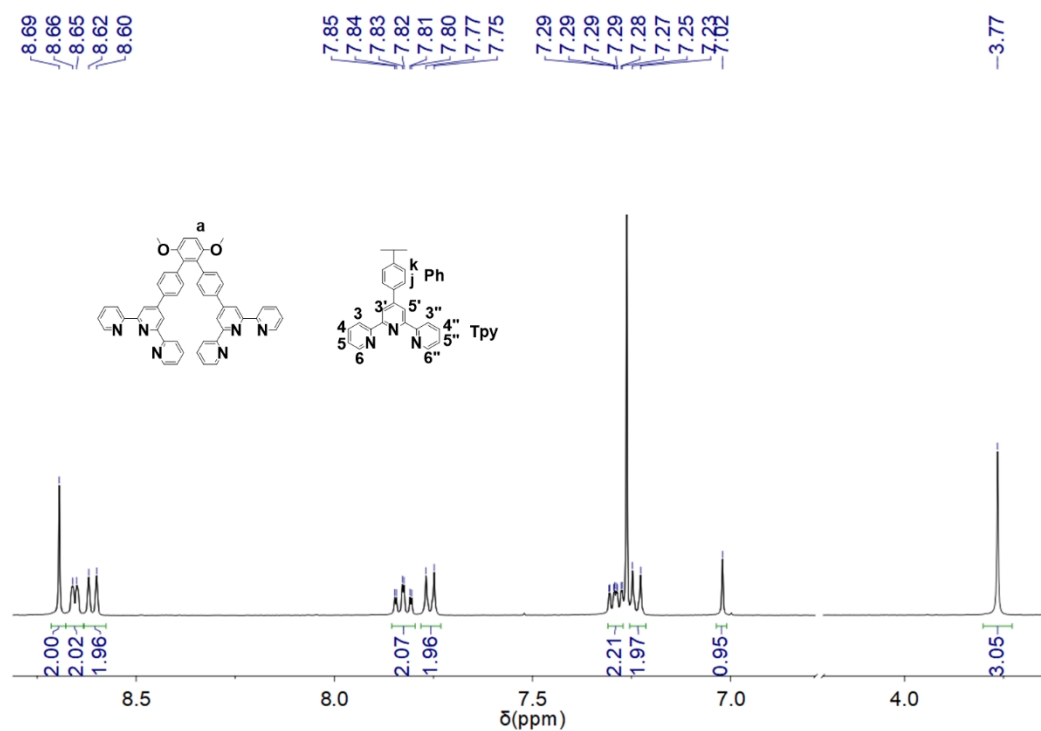
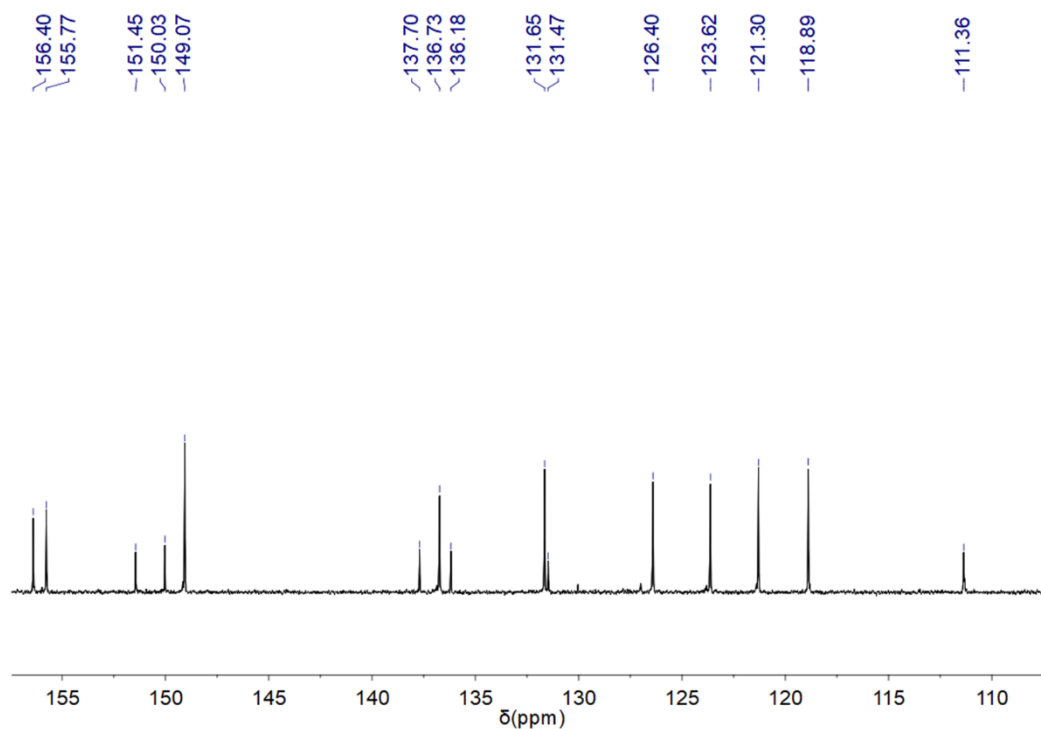**Figure S1.** ^{1}H NMR spectrum (400 MHz, 298 K) of ligand **1** in CDCl$_3$.

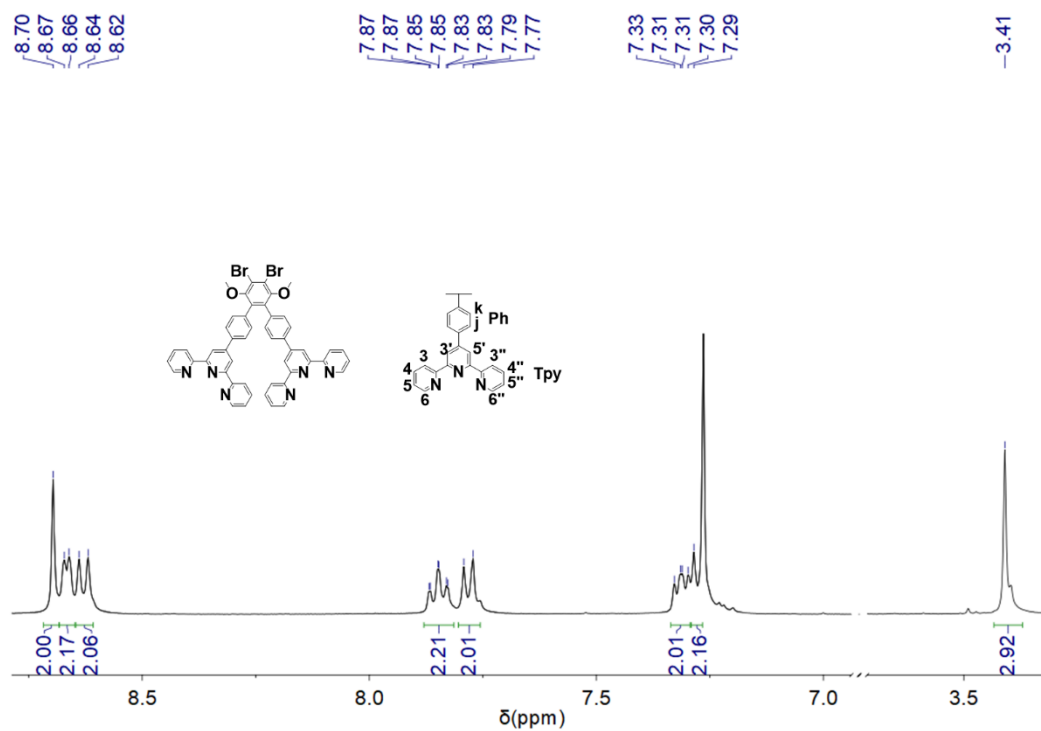**Figure S2.** ^{13}C NMR spectrum (400 MHz, 298 K) of ligand **1** in CDCl$_3$.

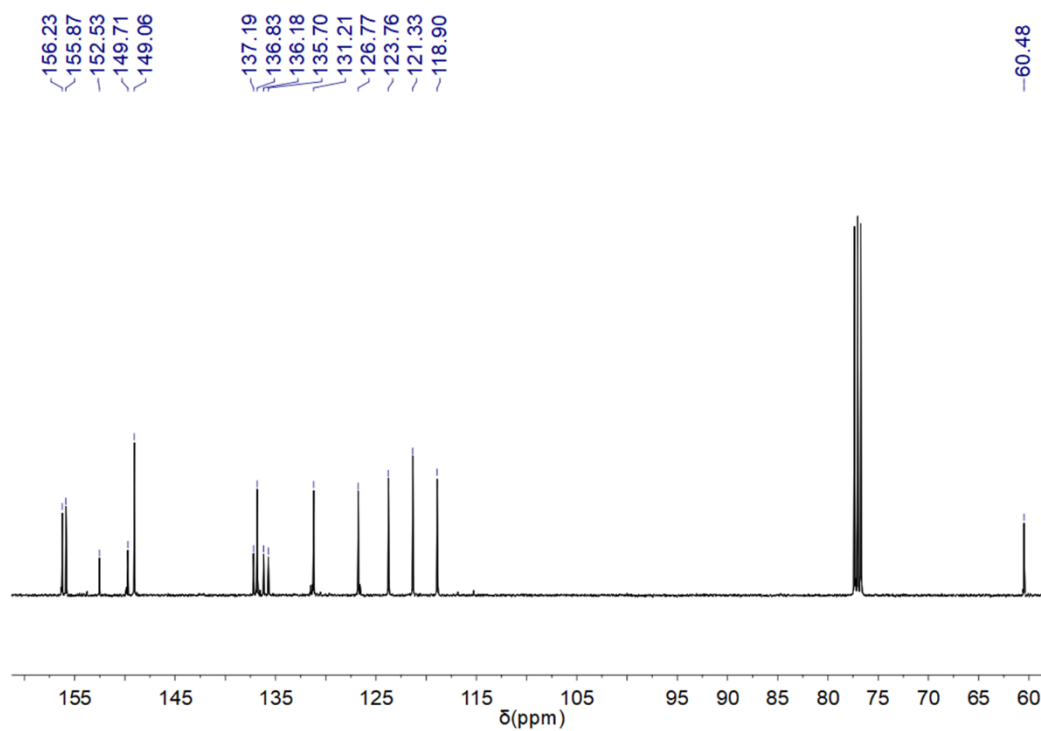**Figure S3.** 1H NMR spectrum (400 MHz, 298 K) of ligand **2** in CDCl3.

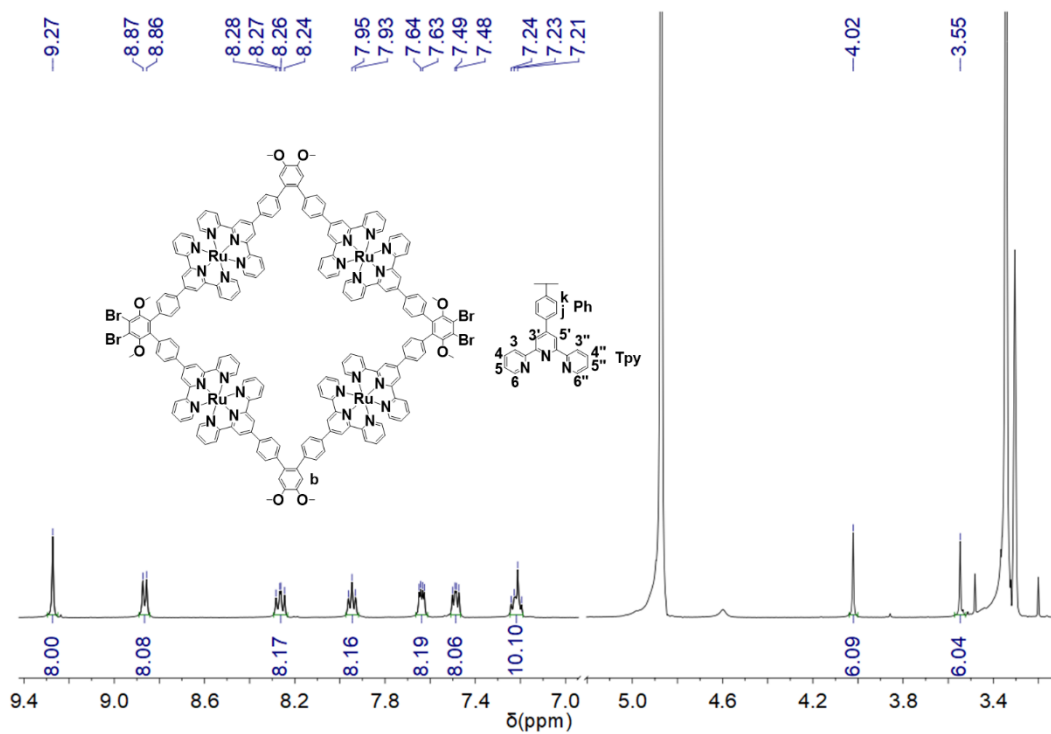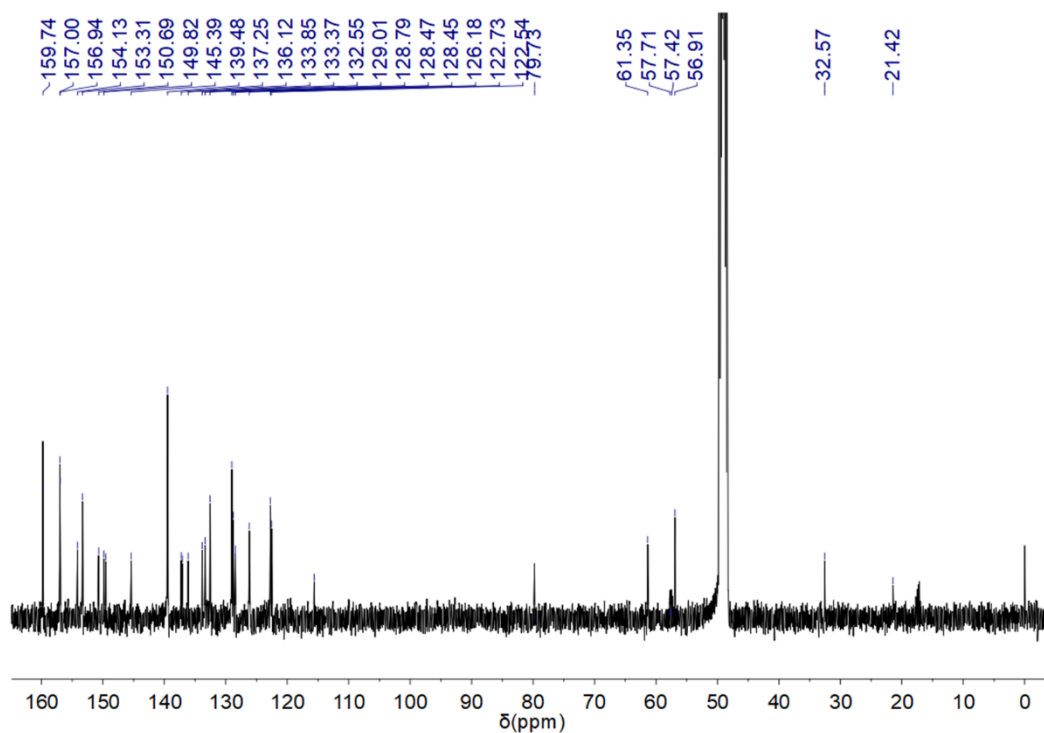**Figure S4.** ^{13}C NMR spectrum (400 MHz, 298 K) of ligand **2** in CDCl$_3$.

Figure S5. ^{1}H NMR NMR spectrum (500 MHz, 298 K) of ligand **4** in CD$_3$OD.

Figure S6. ^{13}C NMR spectrum (400 MHz, 298 K) of ligand **4** in CD$_3$OD.
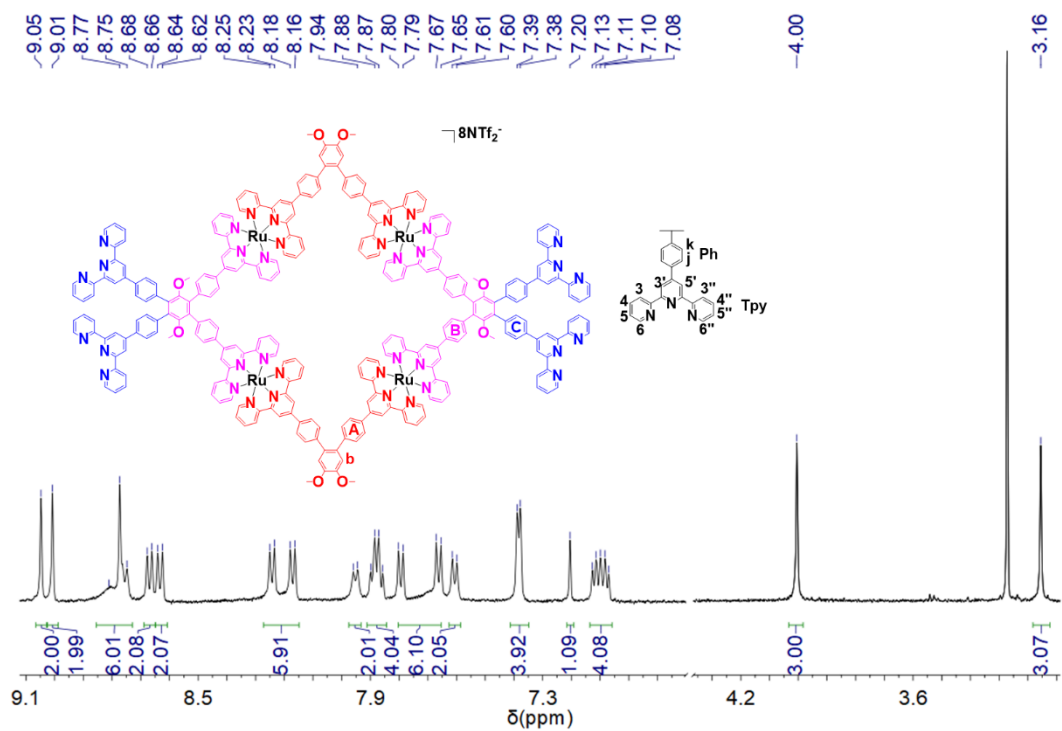
Figure S7. ^{1}H NMR NMR spectrum (500 MHz, 298 K) of ligand **5** in CD$_3$CN.

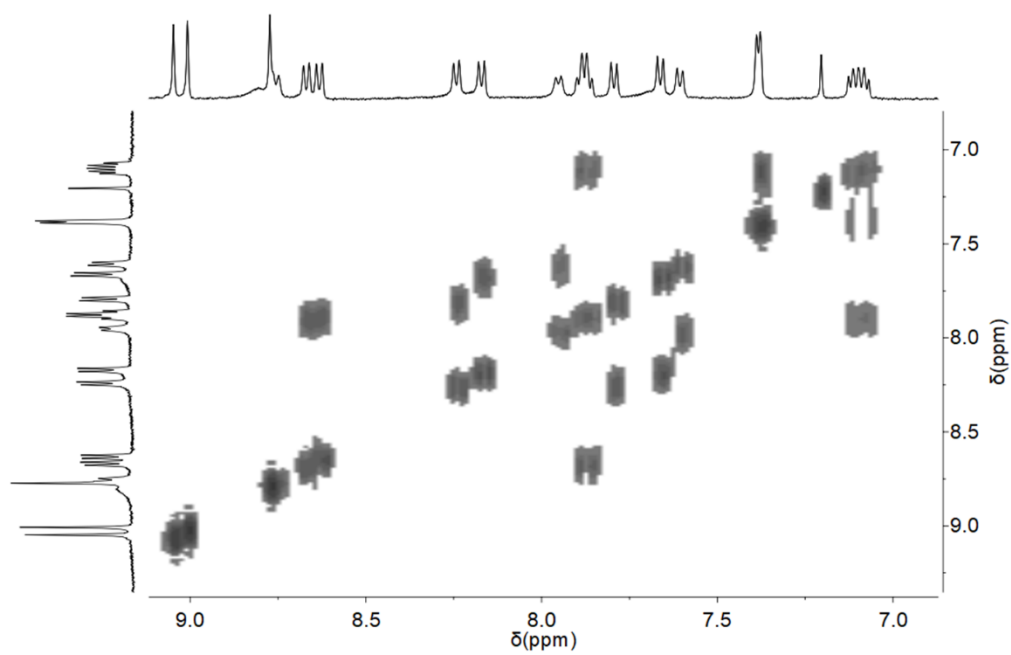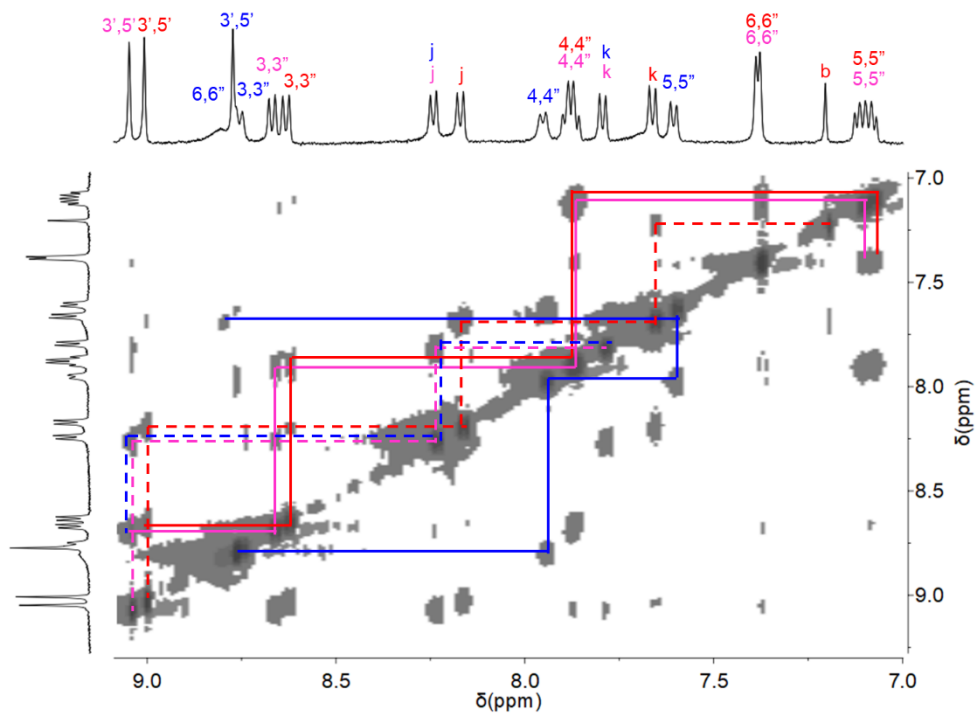**Figure S8.** 2D COSY spectrum (500 MHz, 298 K) of ligand **5** in CD$_3$CN.

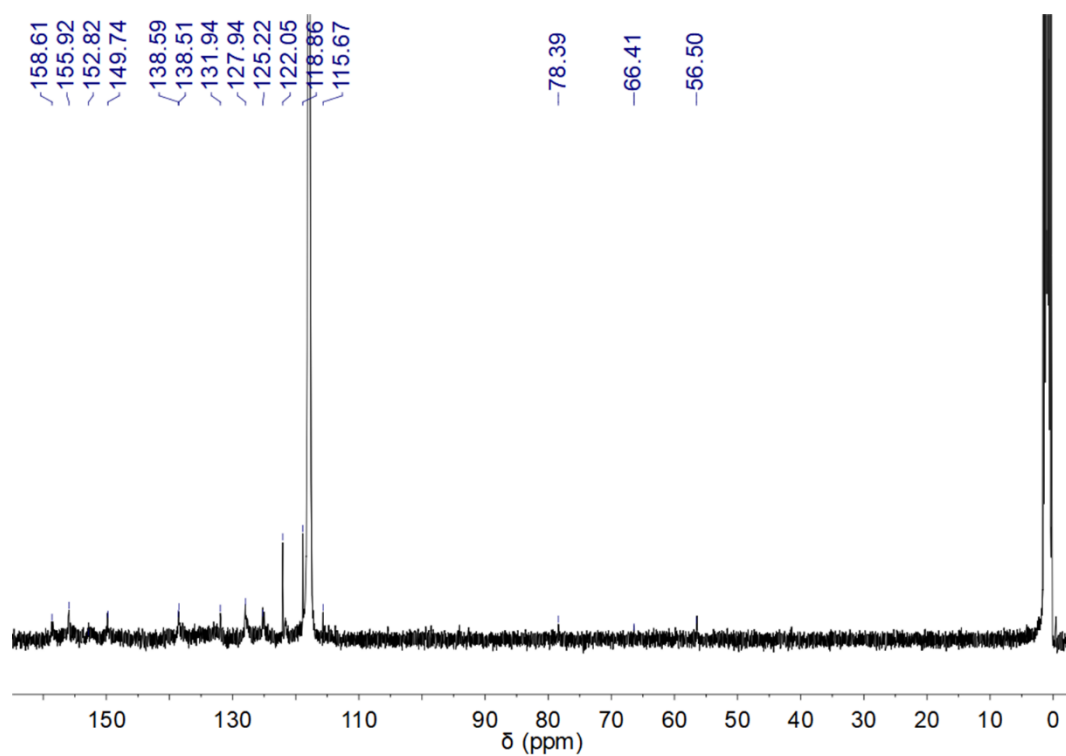**Figure S9.** 2D NOESY spectrum (500 MHz, 298 K) of ligand **5** in CD$_3$CN.

Figure S10. ^{13}C NMR spectrum (400 MHz, 298 K) of Ligand **5** in CD$_3$CN.

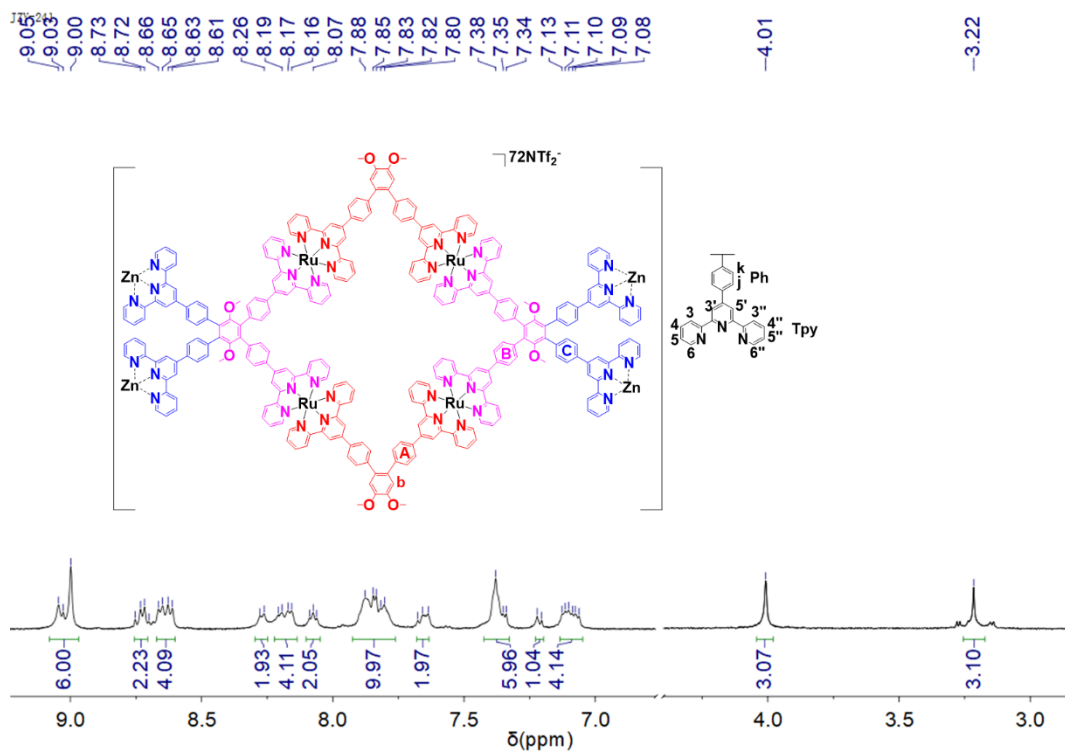**Figure S11.** ^{1}H NMR spectrum (500 MHz, 298 K) of the dendritic-faced metallo-octahedron **6** in CD$_3$CN.
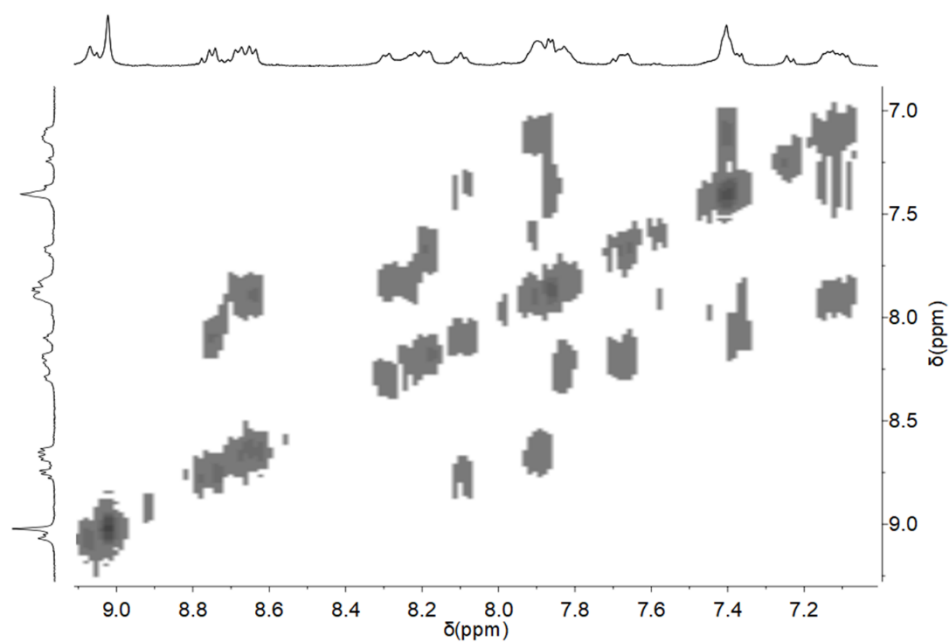

Figure S12. 2D COSY spectrum (500 MHz, 298 K) of the dendritic-faced metallo-octahedron **6** in CD$_3$CN.
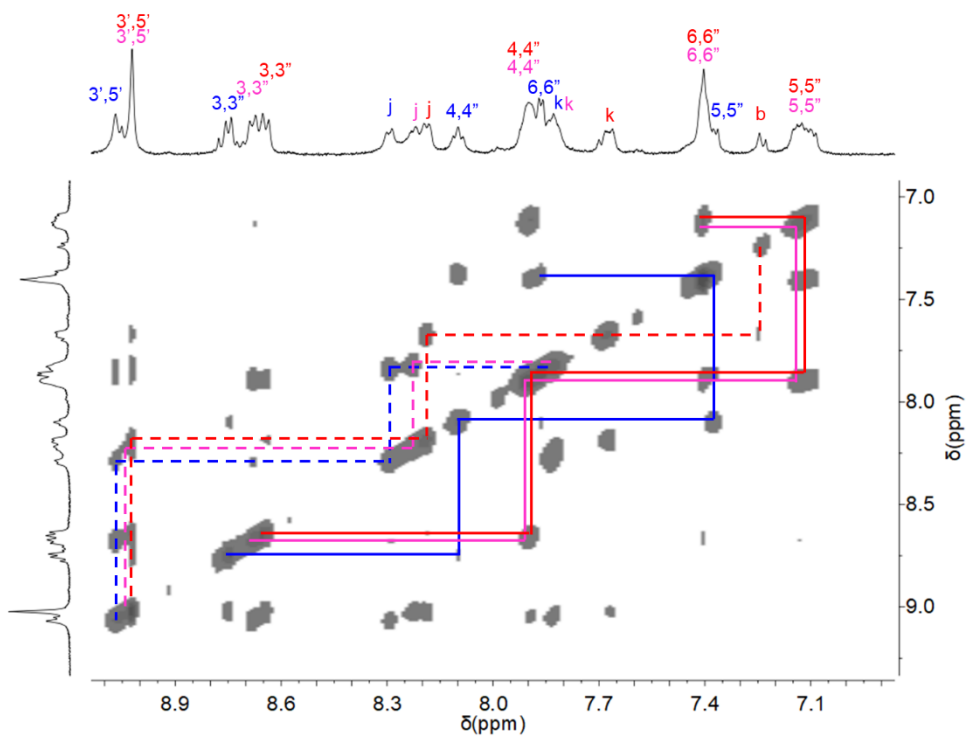
Figure S13. 2D NOESY spectrum (500 MHz, 298 K) of the dendritic-faced metallo-octahedron **6** in CD_3CN.

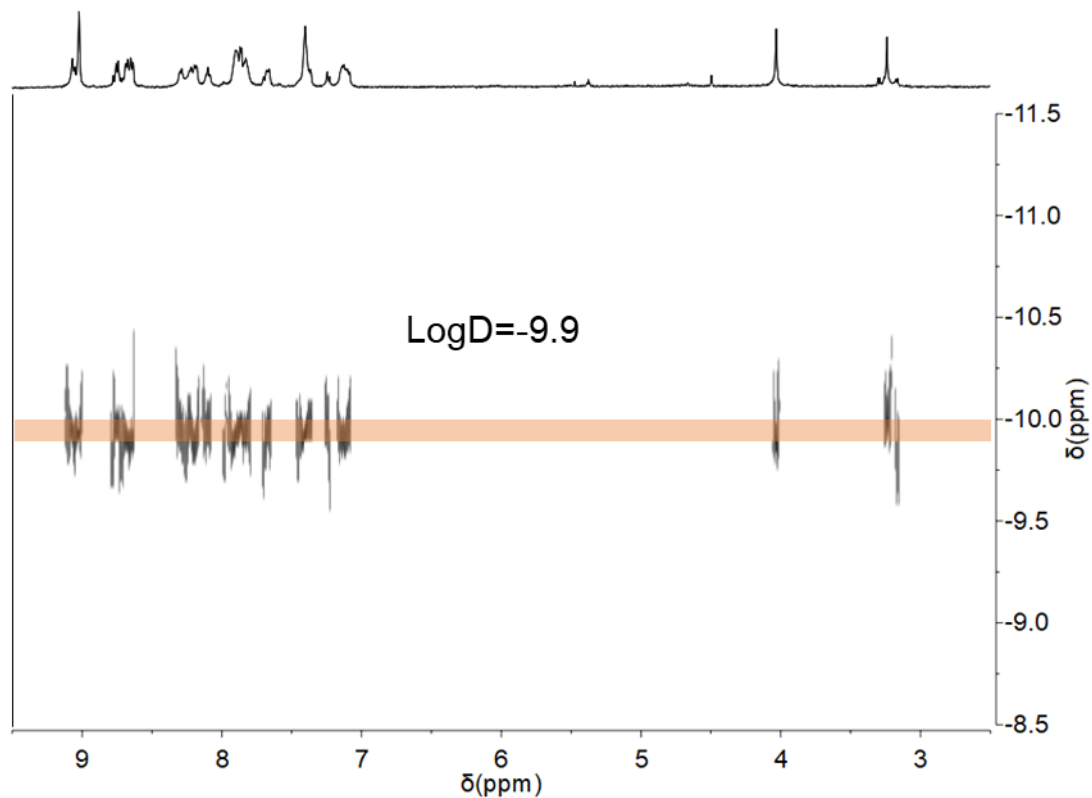**Figure S14.** 2D DOSY spectra (500 MHz) of the dendritic-faced metallo-octahedron **6** in CH_3CN.

4. ESI-MS spectrum of ligand and the dendritic-faced metallo-octahedron 6

1+
753.26

500   750   1000   1250   *m/z*
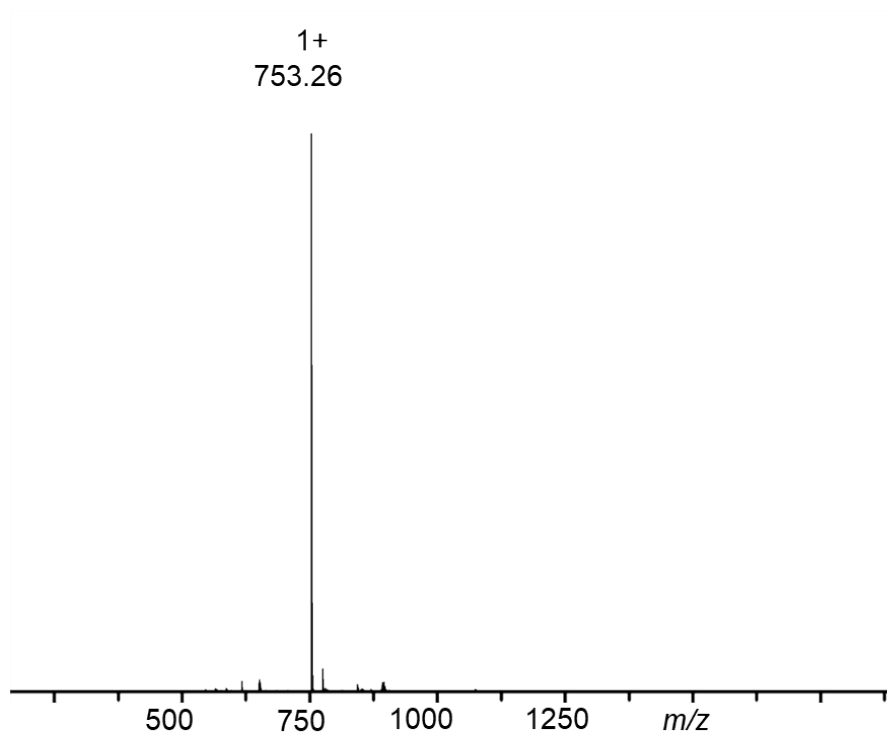
Figure S15. The ESI-MS spectrum of ligand **1.**

1+
911.12

500   750   1000   1250   1500   1750   *m/z*
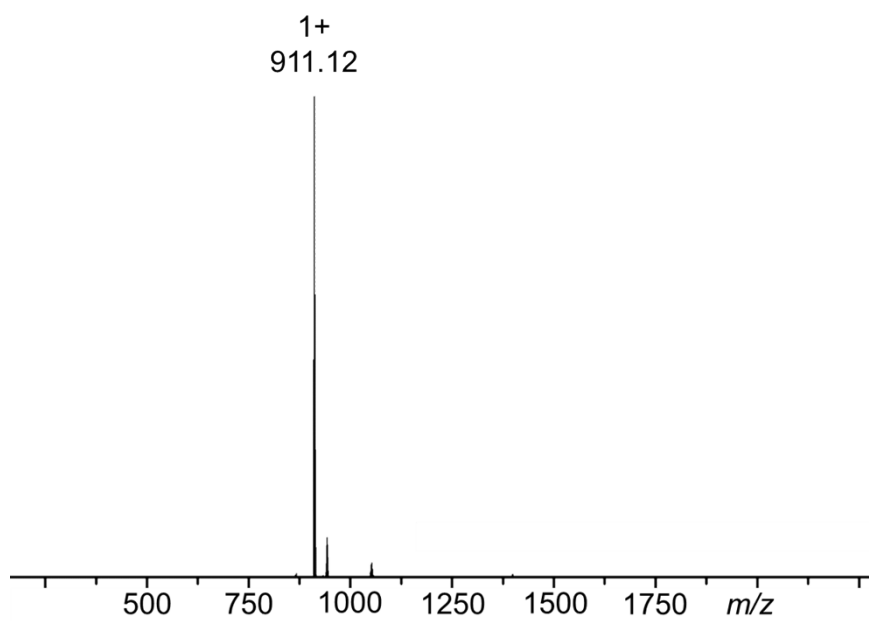
Figure S16. The ESI-MS spectrum of ligand **2.**

Figure S17. The ESI-MS spectrum of ligand **4.**
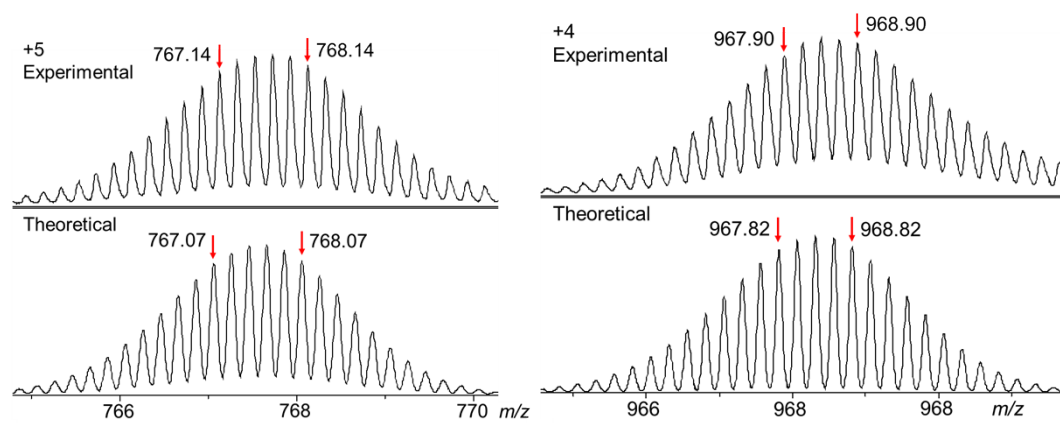
Figure S18. Isotope patterns for the different charge states observed from ligand **4.**

Figure S19. The ESI-MS spectrum of ligand **5.**
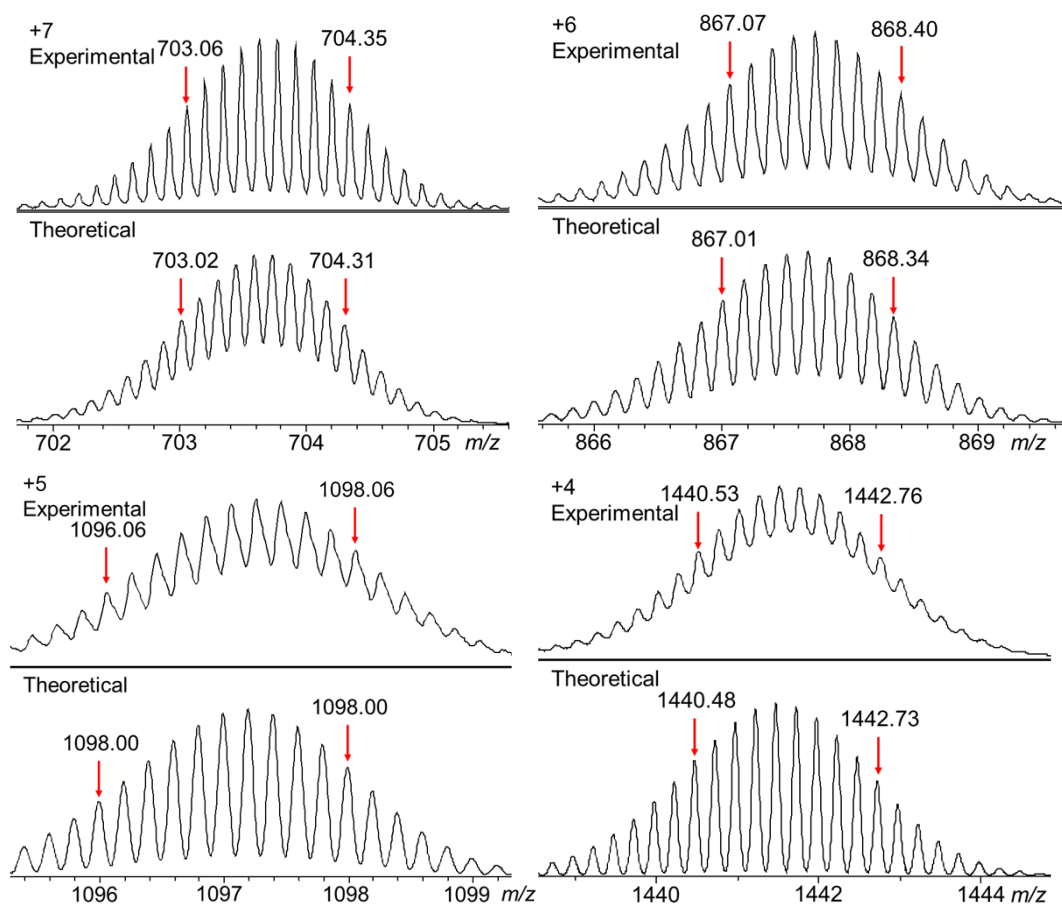
Figure S20. Isotope patterns for the different charge states observed from ligand **5.**

Table S1. The observed and theoretical *m/z* values of ESI-MS for the fragmentations of the dendritic-faced metallo-octahedron **6** (PF_6^- as counterion).

Charge states	Theoretical *m/z*	Experimental *m/z*
28+	1251.21	1251.47
27+	1302.92	1303.04
26+	1358.61	1358.81
25+	1418.75	1419.04
24+	1483.91	1483.98
23+	1554.73	1554.85
22+	1631.99	1632.09
21+	1716.61	1716.98
20+	1809.69	1810.14
19+	1912.57	1912.75
18+	2026.88	2027.27
17+	2154.64	2154.91
16+	2298.36	2298.88
15+	2461.25	2461.30
14+	2647.42	2648.00
13+	2862.22	2862.70

Table S2. The observed and theoretical *m/z* values of ESI-MS for the fragmentations of the dendritic-faced metallo-octahedron **6** (NTf_2^- as counterion).

Charge States	Theoretical *m/z*	Experimental *m/z*
28+	1463.64	1463,92
27+	1528.22	1527.58
26+	1597.77	1597.50
25+	1672.88	1672.83
24+	1754.26	1754.04
23+	1842.71	1842.67
22+	1939.21	1939.25
21+	2044.89	2044.85
20+	2161.14	2161.13
19+	2289.63	2289.77
18+	2432.39	2432.52
17+	2591.95	2592.06
16+	2771.46	2771.23
15+	2974.90	2974.06

Figure S21. Tandem mass spectra of the dendritic-faced metallo-octahedron **6** (PF_6^- as counterion) at trap voltages varied from 15 to 30 V.

5. TEM

9.3 nm

9.5 nm

Figure S22. TEM of the dendritic-faced metallo-octahedron **6**.

Figure S23. TEM image and TEM mapping images of metallo-octahedron.

6. UV-vis and Fluorescence spectrum of the dendritic-faced metallo-octahedron 6

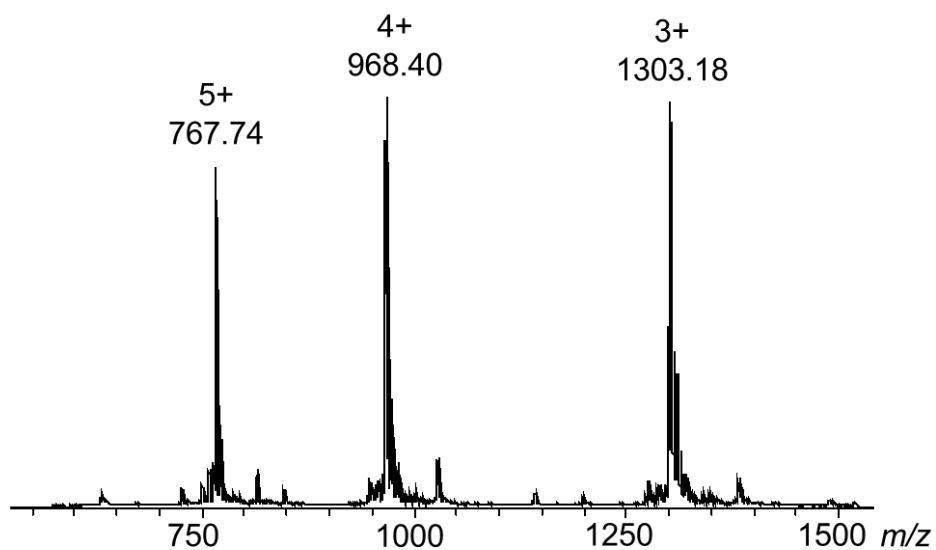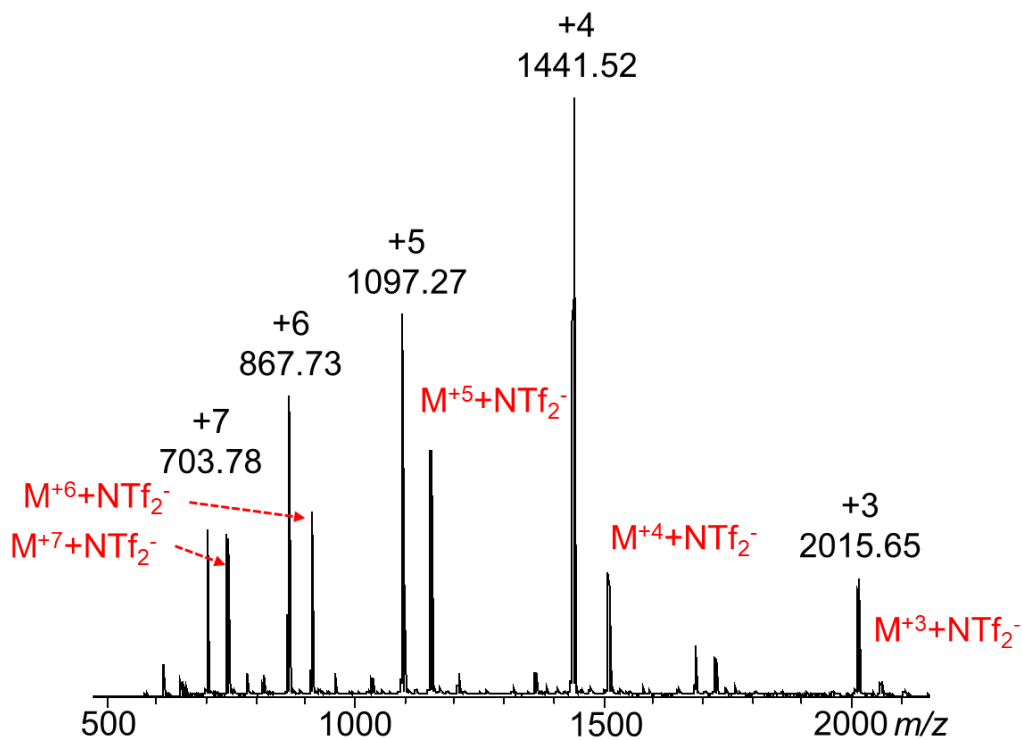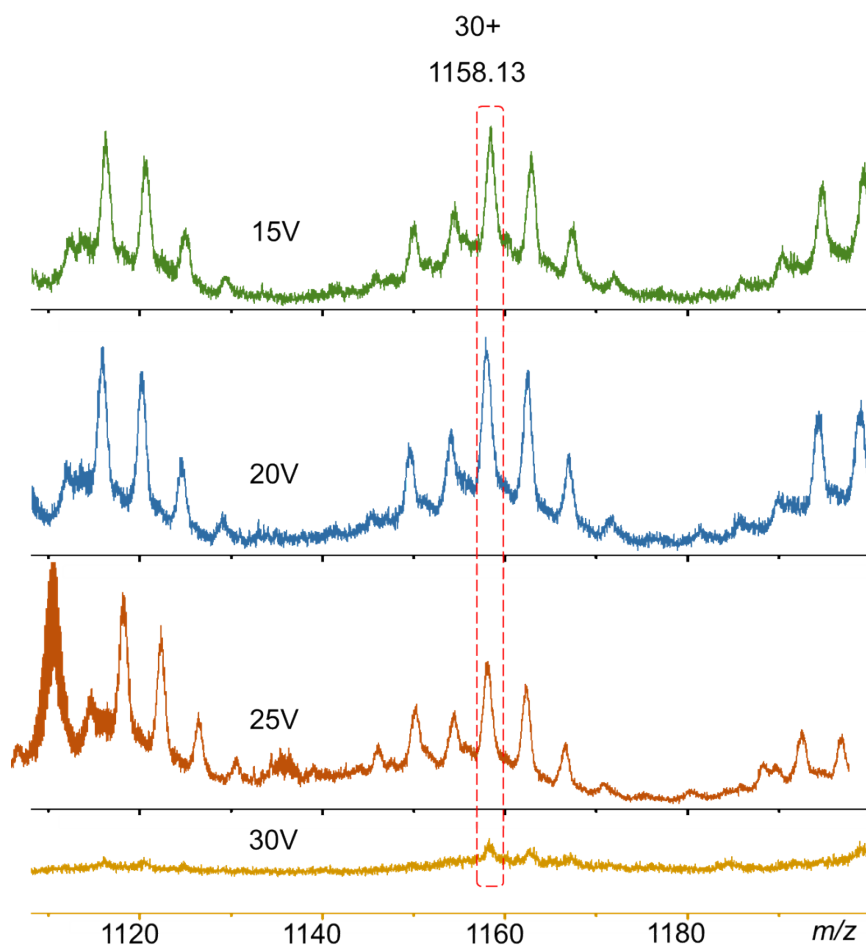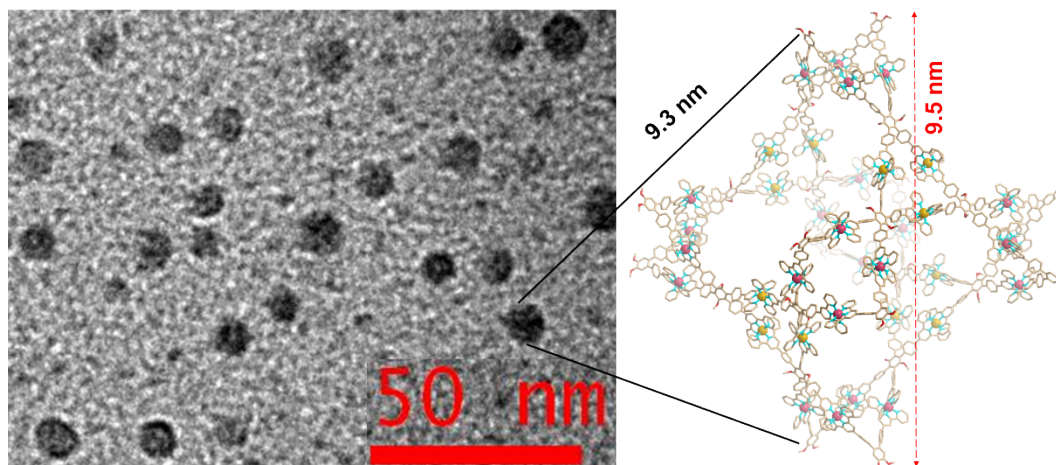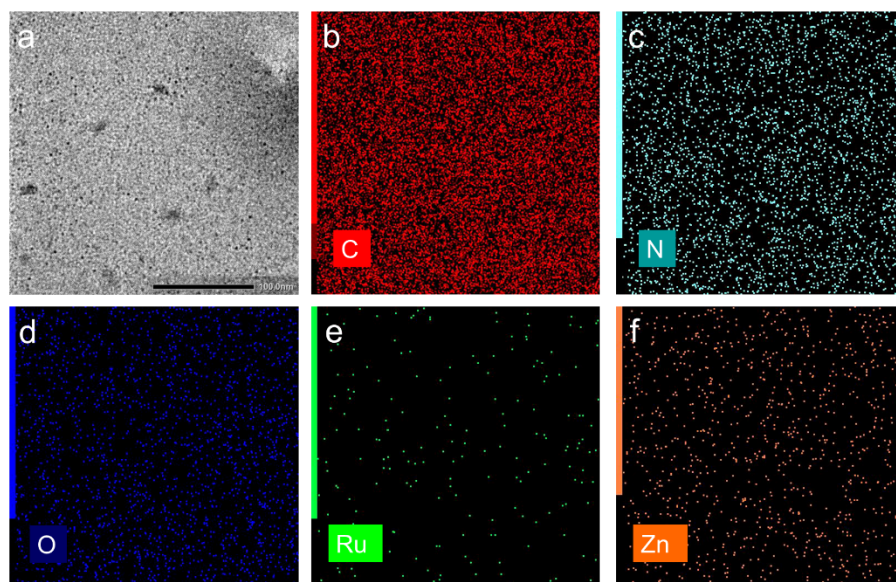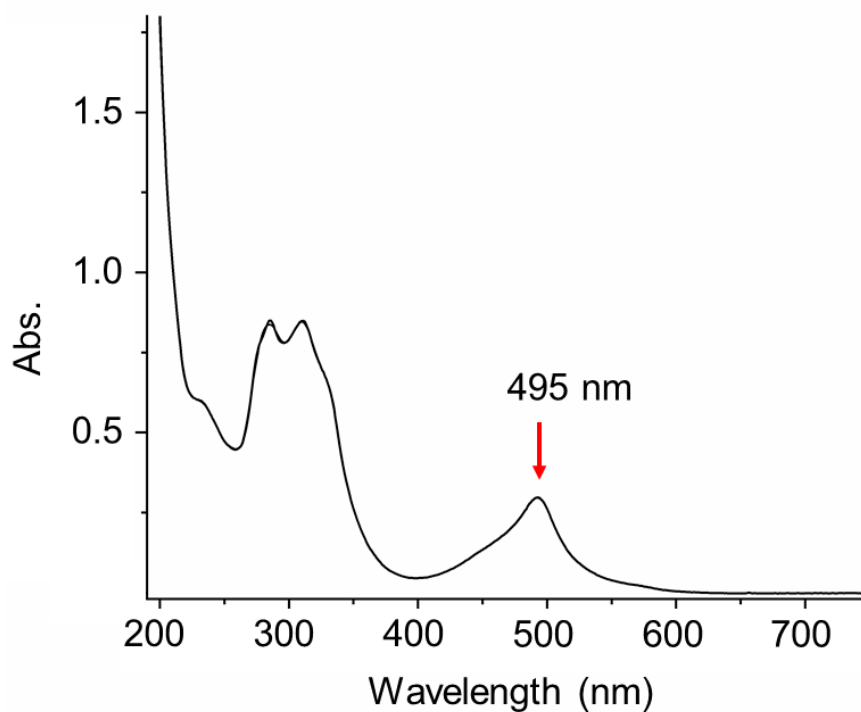Figure S24. UV-vis spectrum of the dendritic-faced metallo-octahedron **6**.
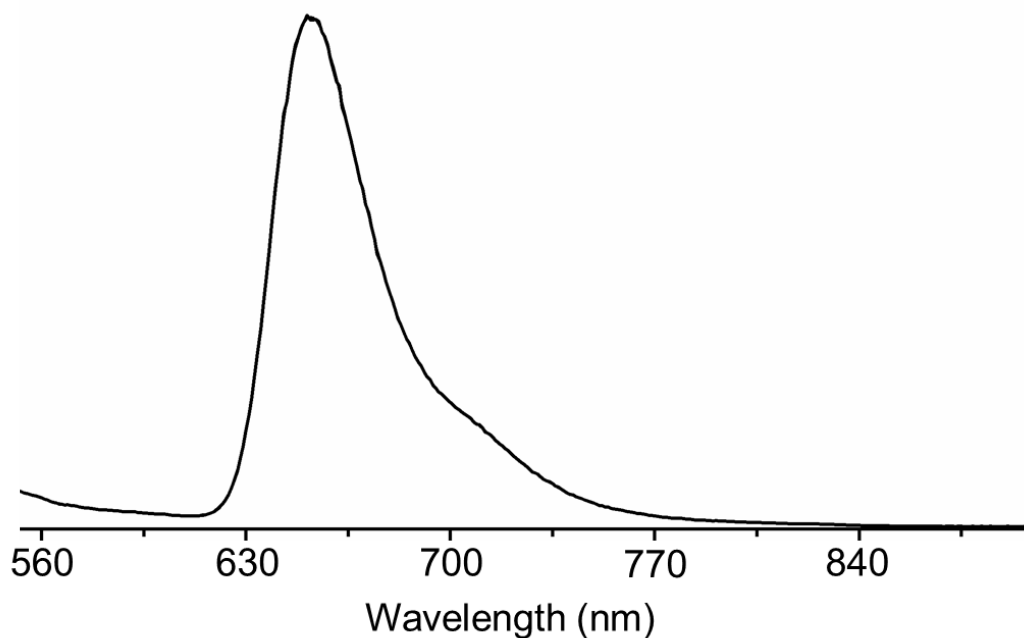
Figure S25. Fluorescence spectrum of the dendritic-faced metallo-octahedron **6**. (λ_{exc} = 495 nm, at 77 K)

7. Detection of $^1O_2$ Generation:

1. 4-oxo-TMP

  2,2,6,6-Tetramethyl-4-piperidone (4-oxo-TMP) was used as a probe to spin trap $^1O_2$ and afford stable 4-oxo-2,2,6,6-tetramethyl-1-piperidinyloxy (4-oxo-TEMPO), which can be detected via electron spin resonance (ESR) spectroscopy.
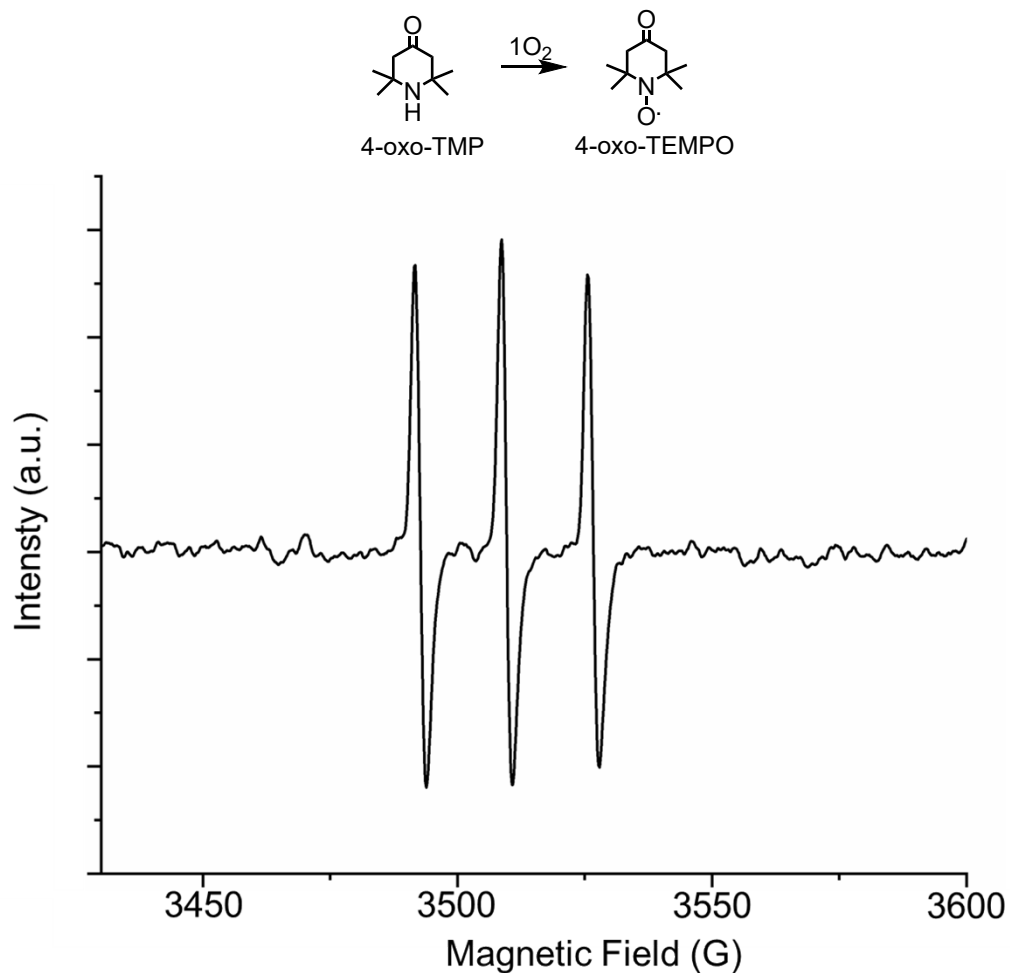
Figure S26. ESR spectra of the dendritic-faced metallo-octahedron **6** mixed with 4-oxo-TMP under visible-light irradiation.

2. DMA

9,10-Dimethylanthracene (DMA) is a fluorescent probe that can be used to detect singlet oxygen production in MeCN. Typically, 2 mg of DMA was dissolved in 4 mL of MeCN with 0.48 μmol $[Ru(tpy)_2](PF_6^-)_2$ or $[Zn(tpy)_2](PF_6^-)_2$ under white LED light irradiation. (ex: 300 nm).
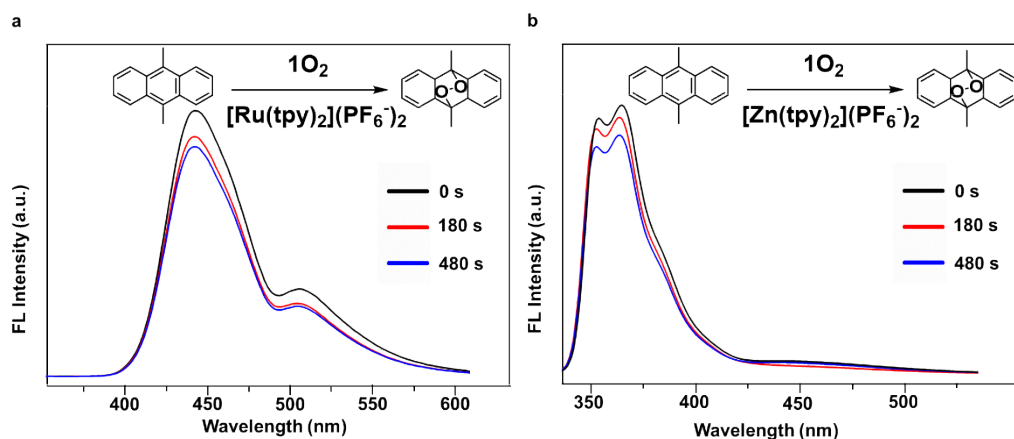
Figure S27. Fluorescence spectra of DMA in the presence of $[Ru(tpy)_2](PF_6^-)_2$ or $[Zn(tpy)_2](PF_6^-)_2$ upon light irradiation.
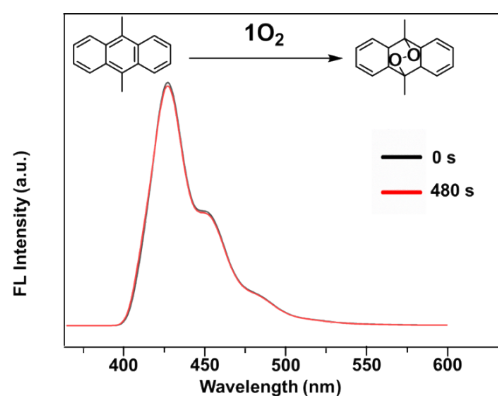
Figure S28. Fluorescence spectra of DMA upon light irradiation.

8. Catalytic Study

the dendritic-faced metallo-octahedron **6** (20.9 mg, 0.43 μmol) was dispersed in 4.5 mL of CD$_3$CN in a sealed glass reactor. After purging with O$_2$ for 10 min, 5 μL (42.8 μmol) of CEES with 0.5 mL CD$_3$CN was added to the glass reactor. After sealing the reactor, it was then exposed to white LED light and monitored by NMR measurement. The product and yield of the reaction was monitored by ^{1}H NMR.
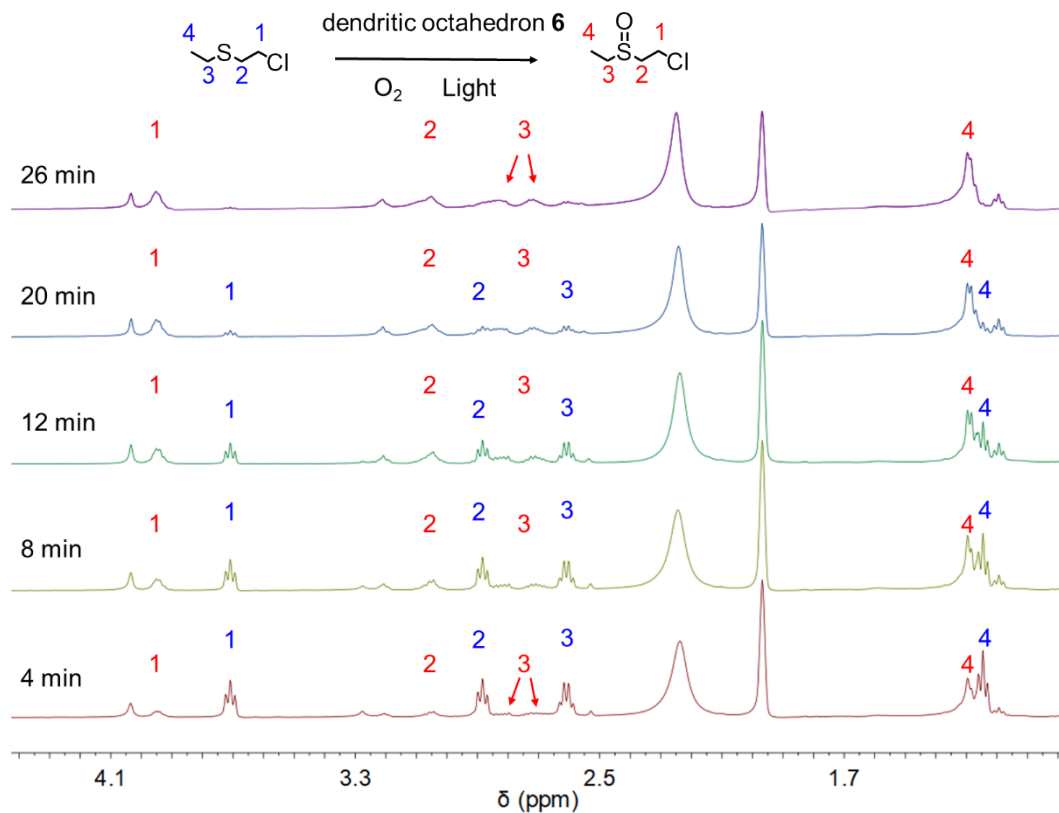
Figure S29. ^{1}H NMR spectra recording the photooxidation reaction of CEES by the dendritic-faced metallo-octahedron **6**.
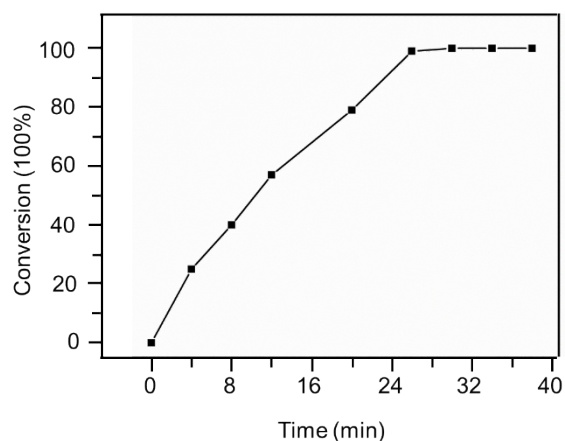
Figure S28. Conversion of CEES in the presence of the octahedron **6** under O$_2$.
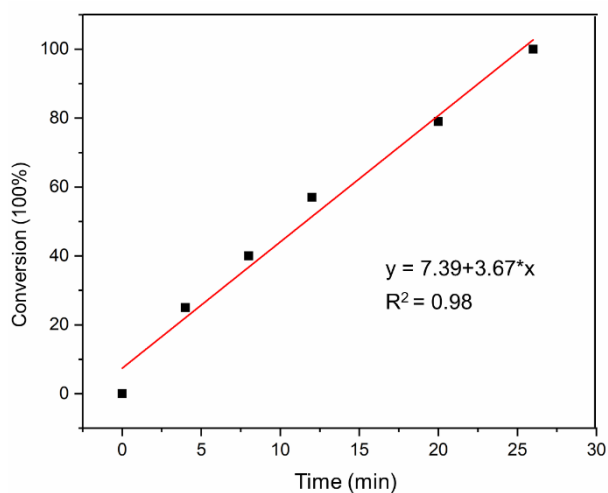
Figure S29. Conversion of CEES in the presence of metallo-octahedron **6** upon light irradiation.

The turn-over frequency (TOF) was calculated by the following formula:

$$TOF = \frac{N_{CEES}}{N_C * T}$$

N_{CEES} is the moles of the substrate (CEES) that are converted in the reaction.

N_C is the moles of the catalyst involved in the reaction.

T is the time to complete the transformation.

Table S3. Kinetic rate constant and TOF values for the catalyst employed in the photooxidation of sulfides.

Catalysis	Kinetic equations	R^2	k (min^{-1})	TOF (min^{-1})
metallo-octahedron	y=7.39+3.67*x	0.98	3.67	3.83

9. TD-DFT Calculations

The HOMO and LUMO of $[Ru(tpy)_2]^{2+}$ held together, while excellent HOMO-LUMO separation can be observed in metallo-octahedron **6**, which favors $^1O_2$ generation [3,4] (Figure S31). In addition, the energy levels of T_3-T_5 are lower than that of S_1 for optimized octahedron **6**, and these energy gaps between S_1 and T_n (n = 3-5) are smaller than 0.3 eV. As to $[Ru(tpy)_2]^{2+}$, only energy levels of T_3–T_4 are lower than that of S_1 (these energy gaps between S_1 and T_n (n = 3–4) are smaller than 0.3 eV). Better HOMO-LUMO separation and more energy transition channels of metallo-octahedron **6** can effectively improve its intersystem crossing (ISC) ability [5,6], which is a critical factor for its photo-activity.

DFT calculations were performed using Gaussian 09 program package[7]. All structures were optimized at the wB97XD level of theory[8] with the def2-SVP basis set[9-10]. The HOMO and LUMO isosurface plots for ground-state structures were computed with Multiwfn 3.8[11] and generated by VMD 1.9.3[12]. The excitation energies for the singlet and triplet states were then evaluated by TD-DFT method at the same level of theory.
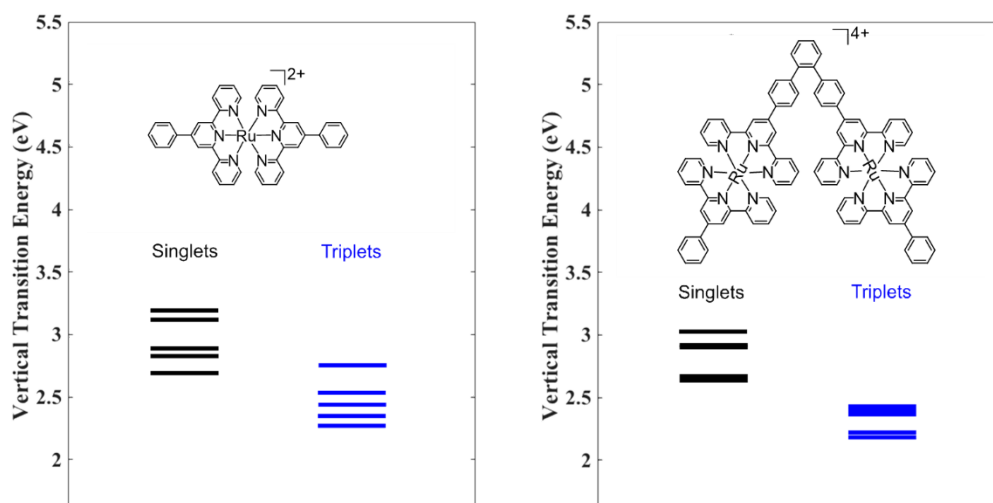

Figure S30. Energy-minimized structures and singlet and triplet energy levels of model compounds of $[Ru(tpy)_2]^{2+}$ and fragment of metallo-octahedron **6**.
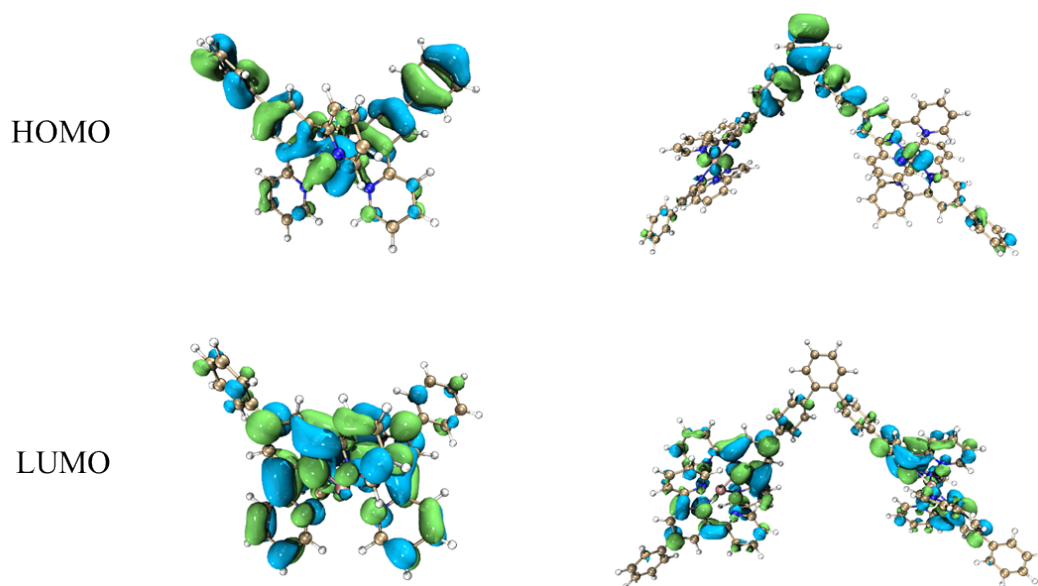
Figure S31. DFT-calculated HOMO and LUMO wave functions of the geometry optimized structures of $[Ru(tpy)_2]^{2+}$ and fragment of metallo-octahedron **6**.

Table S4. The singlet and triplet excited states transition configurations of model $[Ru(tpy)_2]^{2+}$ revealed by TD-DFT calculations.

Structure	Excited state	Excited energy(eV)	[a]Transition configuration(%)
$[Ru(tpy)_2]^{2+}$	S1	2.701	H-1 -> L 94.7%
	S2	2.816	H-1 -> L+3 35.8%, H-1 -> L+10 29.3%, H-1 -> L+5 8.0%, H-1 -> L+1 7.9%
	S3	2.875	H -> L 80.2%, H-6 -> L 9.4%
	S4	3.132	H-1 -> L+3 54.4%, H-1 -> L+10 25.3%
	S5	3.214	H -> L+10 15.9%, H -> L+1 14.5%, H-1 -> L+11 14.1%, H -> L+3 6.8%
	T1	2.258	H-1 -> L+10 58.4%, H-1 -> L+5 11.2%, H-1 -> L+3 6.5%
	T2	2.349	H -> L 69.1%
	T3	2.459	H-1 -> L 49.1%, H -> L+3 22.6%
	T4	2.530	H -> L+3 41.4%, H-1 -> L 26.2%, H-1 -> L+11 6.6%
	T5	2.733	H-1 -> L+3 67.1%, H-1 -> L+10 9.1%

a Only orbit pairs with contribution value greater than 5% are displayed.

Table S5. The singlet and triplet excited states transition configurations of model fragment of metallo-octahedron **6** revealed by TD-DFT calculations.

Structure	Excited state	Excited energy(eV)	[a]Transition configuration(%)
fragment of metallo-octahedron **6**	S1	2.616	H-1 -> L+1 19.8%, H-4 -> L 16.0%, H-4 -> L+1 14.6%, H -> L 12.5%, H-2 -> L 9.3%, H-1 -> L 7.4%
	S2	2.639	H-1 -> L 18.1%, H-5 -> L+1 16.6%, H-5 -> L 15.7%, H-2 -> L+1 12.1%, H -> L+1 8.9%, H-1 -> L+1 6.3%
	S3	2.876	H-4 -> L+7 27.3%, H-1 -> L+7 14.9%, H-4 -> L+5 8.3%, H-2 -> L+7 7.2%, H -> L+7 7.0%
	S4	2.883	H-5 -> L+6 35.9%, H-1 -> L+6 16.7%, H-2 -> L+6 13.9%, H -> L+6 6.4%
	S5	3.012	H-5 -> L+22 18.6%, H-5 -> L+21 11.9%, H-5 -> L+4 7.7%, H-5 -> L+14 6.9%
	T1	2.162	H-1 -> L+1 14.2%, H-1 -> L 13.0%, H -> L 12.1%, H -> L+1 8.8%
	T2	2.189	H-1 -> L 14.0%, H-1 -> L+1 11.7%, H -> L+1 8.3%, H-2 -> L+1 7.6%, H -> L 6.5%, H-2 -> L 5.9%
	T3	2.373	H-1 -> L+7 21.3%, H -> L+7 11.1%, H-2 -> L+7 10.0%, H-1 -> L+5 5.3%
	T4	2.388	H-1 -> L+6 22.0%, H-2 -> L+6 17.7%, H -> L+6 9.2%, H-5 -> L+6 5.1%
	T5	2.409	H-5 -> L+22 23.3%, H-5 -> L+21 14.9%, H-5 -> L+14 6.5%, H-1 -> L+22 5.2%, H-5 -> L+26 5.1%

a Only orbit pairs with contribution value greater than 5% are displayed.

10. Reference

[S1] R. Sarkar, K. Guo, C. N. Moorefield, M. J. Saunders, C. Wesdemiotis and G. R. Newkome *Angew Chem Int Ed,* 2014, **126**, 12378-12381.

[S2] Y.-T. Chan, X. Li, J. Yu, G. A. Carri, C. N. Moorefield, G. R. Newkome and C. Wesdemiotis, *J Am Chem Soc*, 2011, **133**, 11967-11976.

[S3] Y. Yuan, C-J Zhang, M. Gao, R. Zhang, B. Tang, Bin Liu. Specific Light-Up Bioprobe with Aggregation-Induced Emission and Activatable Photoactivity for the Targeted and Image-Guided Photodynamic Ablation of Cancer Cells. *Angew. Chem. Int. Ed.*, 2015, **54**, 1780 –1786.

[S4] S. Xu, Y. Yuan, X. Cai, C.-J. Zhang, F. Hu, J. Liang, G. Zhang, D. Zhang, and B. Liu. Tuning the singlet-triplet energy gap: a unique approach to efficient photosensitizers with aggregation-induced emission (AIE) characteristics. *Chem. Sci.*, 2015, **6**, 5824-5830.

[S5] Q. Zhang, B. Li, S. Huang, H. Nomura, H. Tanaka and C. Adachi. Efficient blue organic light-emitting diodes employing thermally activated delayed fluorescence. *Nature Photonics*, 2014, **8**, 326–332.

[S6] Z. An, C. Zheng, Y. Tao, R. Chen, H. Shi, T. Chen, Z. Wang, H. Li, R. Deng, X. Liu, W. Huang, Stabilizing triplet excited states for ultralong organic phosphorescence. *Nat. Mater.*, 2015, **14**, 685–690.

[S7] M. J. Frisch, G. W. Trucks, H. B. Schlegel, G. E. Scuseria, M. A. Robb, J. R. Cheeseman, G. Scalmani, V. Barone, B. Mennucci, G. A. Petersson, H. Nakatsuji, M. Caricato, X. Li, H. P. Hratchian, A. F. Izmaylov, J. Bloino, G. Zheng, J. L. Sonnenberg, M. Hada, M. Ehara, K. Toyota, R. Fukuda, J. Hasegawa, M. Ishida, T. Nakajima, Y. Honda, O. Kitao, H. Nakai, T. Vreven, J. A. Montgomery, J. E. Peralta, F. Ogliaro, M. Bearpark, J. J. Heyd, E. Brothers, K. N. Kudin, V. N. Taroverov, T. Keith, R. Kobayashi, J. Normand, K. Raghavachari, A. Rendell, J. C. Burant, S. S. Iyengar, J. Tomasi, M. Cossi, N. Rega, J. M. Millam, M. Klene, J. E. Knox, J. B. Cross, V. Bakken, C. Adamo, J. Jaramillo, R. Gomperts, R. E. Stratmann, O. Yazyev, A. J. Austin, R. Cammi, C. Pomelli, J. W. Ochterski, R. L. Martin, K. Morokuma, V. G. Zakrzewski, G. A. Voth, P. Salvador, J. J. Dannenberg, S. Dapprich, A. D. Daniels, O. Farkas, J. B. Foresman, J. V. Ortiz, J. Cioslowski, D. J. Fox. Gaussian 09 (Revision D.01) I. *Gaussian, Wallingford*, *CT*, 2013.

[S8] J.-D. Chai and M. Head-Gordon. Long-range corrected hybrid density functionals with damped atom-atom dispersion corrections. *Phys. Chem. Chem. Phys.* 2008, **10**, 6615-6620.

[S9] F. Weigend and R. Ahlrichs. Balanced basis sets of split valence, triple zeta valence and quadruple zeta valence quality for H to Rn: Design and assessment of accuracy. *Phys. Chem. Chem. Phys.* 2005, **7**, 3297-3305.

[S10] F. Weigend. Accurate Coulomb-fitting basis sets for H to Rn. *Phys. Chem. Chem. Phys.* 2006, **8**, 1057-1065.

[S11] T. Lu, F. Chen. Multiwfn: A multifunctional wavefunction analyzer. J. *Comput. Chem.* 2012, **33**, 580-592.

[S12] W. Humphrey, A. Dalke, K. Schulten., VMD: Visual molecular dynamics. *Journal of molecular graphics* 1996, **14**, 33-38.